AIAA JOURNAL
Vol. 44, No. 3, March 2006

# Wake Control Based on Spanwise Sinusoidal Perturbations

Adrian Dobre,* Horia Hangan,† and Barry J. Vickery‡
*University of Western Ontario, London, Ontario N6A 5B9, Canada*

**The effectiveness of a passive sinusoidal perturbation method, applied on the upstream faces of square cylinders at a wavelength that corresponds to the wavelength of the intermediate wake instability mode, is experimentally investigated. Hot-wire measurements are taken to examine the effect of three different sinusoidal perturbation amplitudes as compared to the straight cylinder case. Good agreement is found between high- and low-Reynolds-number results, suggesting that the main flow dynamics features, as well as the flow control method efficiency, are Reynolds independent. Two sets of measurements are taken: in the near and in the intermediate to far wake. The near-wake measurements show that the method is very effective in mitigating the von Kármán vortices as previously found, whereas the intermediate to far wake measurements indicate that the wake decay is accelerated by the sinusoidal perturbations, therefore, being beneficial in the reduction of wake aeroelastic instabilities.**

## Nomenclature

| | | |
|---|---|---|
| $d$ | = | cylinder width in $y$ direction |
| $f$ | = | frequency |
| $k^2$ | = | hot-wire longitudinal cooling coefficient |
| $L$ | = | cylinder length in $z$ direction |
| $L_{11}$ | = | integral length scale based on $x$-direction velocity |
| $Sr$ | = | Strouhal number |
| $T_{11}$ | = | integral timescale based on $x$-direction velocity |
| $U_0$ | = | $x$-direction freestream velocity |
| $u$ | = | $x$-direction velocity |
| $u'$ | = | $x$-direction velocity standard deviation |
| $v$ | = | $y$-direction velocity |
| $v'$ | = | $y$-direction velocity standard deviation |
| $w$ | = | $x$-direction amplitude |
| $\lambda$ | = | $z$-direction wavelength |
| $\lambda_x$ | = | $x$-direction wavelength |

## I. Introduction

FLOW control, with its incommensurable benefits, optimal use of materials, low costs, increase in safety, and reliability becomes the final target of numerous fluid mechanics investigations. Flow control is defined as "the process or operation by which certain characteristics of a given flow are manipulated in a such a way as to achieve improvements of a specific technical performance."[1] The parameters to be optimized in the wake control applications are the drag force, lift force variance, and the downstream wake mixing and decay. Note that this downstream wake evolution, despite its role in triggering vicious wake aeroelastic instability, has not drawn too much attention in the wake control literature.

Because of their relative simplicity and that they do not require an external energy source, passive control mechanisms are generally preferred over the active devices, and the present work is limited to the former. Among previously investigated passive flow control strategies, the spanwise periodic perturbation method (SPPM) was found to be very efficient and relatively simple to implement on most geometries. The method commonly involves the application of periodic geometric distortions to the leading or trailing edge or the face of the body in question and can result in the suppression of vortex shedding and a reduction of drag force. This is not a trivial result because, for example, the well-known Scruton and Walshe helical strakes method,[2] although successful in suppressing the vortex induced vibration of steel chimneys, produces a substantial increase in drag coefficient and, hence, increases base bending moments.[3]

SPPM is not new in fluid dynamics applications. Reference 4 provides a chronological review of these applications. SPPM was first applied by Naumann et al.[5] They showed that the vortex shedding could be suppressed by applying step changes in the separation line along the span of a circular cylinder at a supercritical Reynolds number of $5 \times 10^5$. Later, Tanner[6] applied a similar step change to the blunt trailing edge of a winglike profile. He recorded a significant increase in the pressure at the trailing edge associated with a decrease in the drag coefficient of up to 64%. The segmented trailing-edge studies were successfully continued in Refs. 7–9. However, these studies were largely exploratory, and no explanations of the fluid dynamics phenomena that result the beneficial effect of SPPM were given.

Later, Bearman and Tombazis[10] and Tombazis and Bearman[11] experimentally investigated the three-dimensional features of the high Reynolds number ($Re = 4 \times 10^4$) wake behind half-ellipse models with a sinusoidal type of SPPM applied at its blunt trailing edges. Similar to previous investigations, the authors found a significant decrease in the drag coefficient of up to 34%. Based on spectral analysis in the near wake, they speculated that the decrease in the drag coefficient was mainly due to the vortex dislocations introduced by wake generator waviness. In a follow up work, Bearman and Owen[12] investigated the effect of the sinusoidal perturbation method applied on the leading edge of a square cylinder and on flat plates, that is, implying waviness at both the leading and trailing edges, at a high Reynolds number of $4 \times 10^4$. The authors considered six different sinusoidal perturbations configurations (combining three sinusoidal amplitudes and four spanwise wavelengths) and found that mild perturbations with wave steepness $w/\lambda$, where $w$ is the sinusoidal amplitude and $\lambda$ is the spanwise wavelength (Fig. 1), of 0.06–0.09 lead to a complete suppression of the vortex shedding along with a decrease in the drag coefficient of up to 30% or more. Note that the four wavelengths $\lambda$ were chosen rather arbitrarily, between $3.5d$ and $5.6d$, where $d$ is the transverse cross-section edge of the cylinder (Fig. 1). These wavelengths are comparable to the typical vortex shedding spanwise correlation lengths found by Vickery[13] based on pressure measurements on the wake generator.

Darekar and Sherwin[4] performed a direct numerical simulation (DNS) of the wavy square cylinders with the aim to give further insight into the dynamics of coherent structures responsible for the beneficial effects of sinusoidal perturbations. Most of their

Received 22 December 2004; revision received 16 August 2005; accepted for publication 27 September 2005. Copyright © 2005 by the American Institute of Aeronautics and Astronautics, Inc. All rights reserved. Copies of this paper may be made for personal or internal use, on condition that the copier pay the $10.00 per-copy fee to the Copyright Clearance Center, Inc., 222 Rosewood Drive, Danvers, MA 01923; include the code 0001-1452/06 $10.00 in correspondence with the CCC.

*Research Associate, Department of Civil and Environmental Engineering; currently Postdoctoral Research Fellow, Department of Meteorology, School of Mathematics, Meteorology and Physics, University of Reading, Earley Gate, Reading, England RG6 6BB, United Kingdom; a.dobre@rdg.ac.uk.

†Associate Professor and Associate Research Director, Boundary Layer Wind Tunnel Laboratory, Faculty of Engineering.

‡Professor Emeritus and Research Director, Boundary Layer Wind Tunnel Laboratory, Faculty of Engineering.

simulations were performed at a low Reynolds number of 100. They proposed two parameters, wave steepness $w/\lambda$ and normalized wavelength $\lambda/d$, as governing parameters of the flow around wavy cylinders. These authors found three distinct regimes in the plane defined by these two parameters ($w/\lambda$ and $\lambda/d$) (Fig. 2) : 1) regime 1 that is similar to the straight cylinder configuration, that is, the waviness effects are negligible; 2) regime 2, a regime of transition, characterized by a decrease in lift variance of up to 50% along with a small (4.5%) decrease in drag coefficient; and 3) regime 3, with a complete suppression of the vortex shedding along with a significant drag reduction of up to 16.8%. It was suggested that the simultaneous reduction in drag coefficient and vortex shedding mitigation could be attributed to the development of shear-layer three dimensionality. This makes them less susceptible to rolling up into a von Kármán vortex street by diverting roll spanwise vorticity into ribs streamwise and vertical vorticity components. The three-dimensional vorticity may divert the interaction between the two shear layers and, hence, suppress the von Kármán street formation. Because their numerical results indicate that the most significant reduction in the lift variance and drag coefficient is obtained for small wave steepness at a wavelength of $5.5d$, that is, close to the $5.22d$ wavelength of the laminar wake instability mode $A$, identified in the straight square cylinders,[14] the authors also speculate that the wavy cylinders might trigger the development of the wake instability mode $A$, originally found in straight circular cylinders.[15] Moreover, based on vorticity contours, Darekar and Sherwin[4] showed that in regime 2 the near-wake topology does display a resemblance to mode $A$ topology.

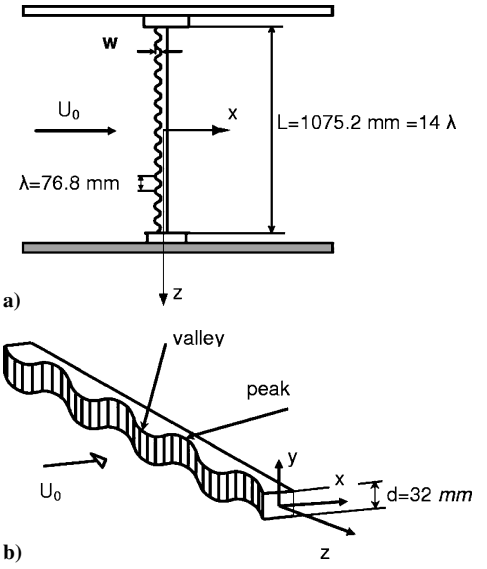


**Fig. 1 Experimental arrangement: a) upper view and b) three-dimensional view.**

Note the good agreement between the experimental high-Reynolds-number results[12] and the DNS, low-Reynolds-number results.[4] For example, in both laminar and turbulent regimes, a normalized wavelength $\lambda/d$ of approximate 5.5 is the most unstable because it gives maximum control benefits for small wave steepness ratios. Moreover, at both high and low Reynolds numbers, the sinusoidal perturbation method was found to be effective in reducing the drag and in suppressing the vortex shedding. However, based on the existing literature, a complete similarity between the two regimes cannot be stated because the experimental data at high Reynolds numbers is available only for relatively high spanwise wavelength waviness (between $3.5d$ and $5.5d$) and only for six configurations, all of them corresponding only with the aforementioned laminar regime 3 (Fig. 2). Therefore, more experimental evidence is needed to assess the legitimacy of the extension of the low-Reynolds-number results to the high-Reynolds-number applications for the flow around wavy cylinders. For example, to clarify the similarity between the laminar and turbulent cases, it would be of interest to investigate if the three wavy cylinder regimes found in the laminar case are present in the turbulent case.

The previous investigations mentioned focused on the SPPM effect on the wake generator itself; therefore, only near wake measurements were considered. Thus, only the effects on the drag coefficient and lift force variance were considered. However, also of interest is the wake decay farther downstream, the third wake control parameter to be optimized that is not necessarily related to the first two.[16] Moreover, the results in Refs. 17 and 18 suggest a farther downstream reorganization of the wake for other types of control methods. This reorganization could lead to further aeroelastic interactions in the wake. To our knowledge, there is no published material to address this problem for SPPM. Because Dobre and Hangan[19] and Dobre[20] showed that a turbulent mode $A$ with a spanwise wavelength of $2.4d$ is responsible for the significant decay of the von Kármán vortices through the interactions with the secondary structures, it is of interest to investigate the effect of this particular wavelength on the downstream wake decay.

The objectives of the present work are 1) to relate the sinusoidal SPPM to the preferential intermediate wake instability mode $A$, 2) to further explore the control parametric space defined by Darekar and Sherwin[4] and to document the comparison between the low and high-Reynolds-number sinusoidal SPPM, and 3) to investigate the farther downstream effect of the sinusoidal SPPM on the wake decay.

## II. Experimental Description

Three wavy aluminum bars were machined from a square cylinder with the cross-sectional edge $d = 32$ mm such as the upstream faces to be sinusoidal (Fig. 1). Note that this setup is similar to the

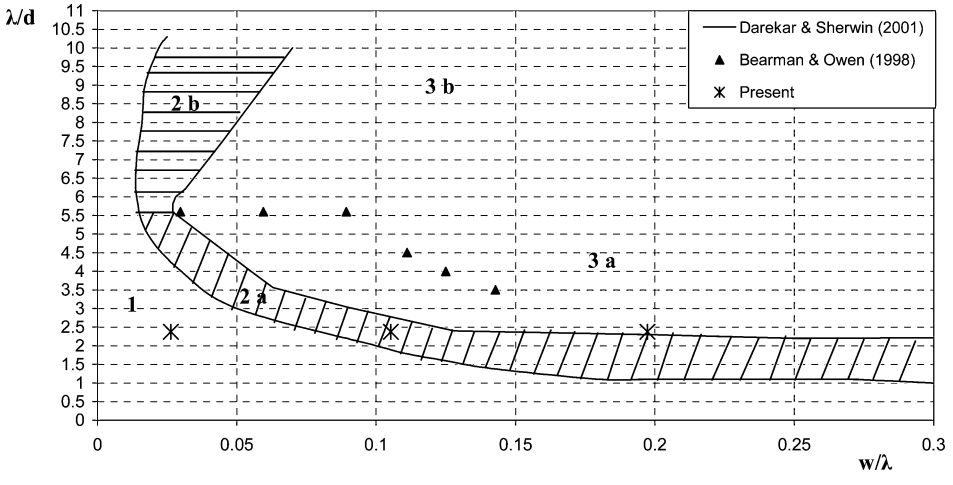


**Fig. 2 Wavy square cylinders flow regimes.**

configuration by Bearman and Owen.[12] To investigate the effect of the waviness, a straight square cylinder with a 32-mm edge was also considered as the base case. The wavy cylinders have normalized spanwise perturbation wavelength $\lambda/d$ of 2.4. The sinusoidal amplitudes $w/d$ were chosen as 2/32, 8/32, and 15/32, corresponding to wave steepness factors $w/\lambda$ of 0.026, 0.105, and 0.197. (These configurations will be referred hereafter as $w1$, $w2$, and $w3$, respectively, and the base case will be referred as $w0$.) Note that, herein, we adopt the waviness peak and valley definitions introduced in Ref. 12 and indicated in Fig. 1. The cylinders were mounted under adequate tension between two end plates to ensure that they were straight and rigid. The two end plates were set parallel to one another at a distance $L$ of 1075.2 mm ($=14\lambda$) that gives a relatively high aspect ratio $L/d$ of 33.6. Note that no end effects control methods[15] have been applied during the measurements.

The experiments were performed at the Boundary Layer Wind Tunnel Laboratory located at the University of Western Ontario, London, Ontario, Canada. The wind tunnel is a boundary-layer tunnel with an open-return suction circuit. The total length of the tunnel is 33 m, but only the upstream section of the tunnel was used to avoid interferences with the downstream development of the boundary layer.

At the location where measurements were taken, the wind-tunnel section was rectangular with the dimensions $1.7 \times 2.4$ m. The streamwise turbulence intensity was less than 0.5%, and the cross-stream turbulence intensities were less than 0.3%. The wind-tunnel reference velocity was monitored throughout the experiment and kept constant at 11 m/s using a pitot tube connected to an electronic manometer. The Reynolds number based on $d$ and on the freestream velocity $U_0$ was $2.35 \times 10^4$. The longitudinal integral timescale $T_{11}$ is 6 ms, and the integral length scale, based on the Taylor hypothesis that assumes the convective velocity equal to the freestream velocity, is approximately $L_{11} = 70$ mm. No particular peaks have been found in the power spectra of all velocity components. The temperature in the wind tunnel did not vary more than 0.5°C during the experiments due to a temperature-controlled environment. The tunnel walls were adjusted to set the axial pressure gradient to zero, with a variation of less than 1% along the measurement stations. Measurements of the velocity profiles indicate that the velocity was uniform within 1%.

Velocity measurements were taken using a DANTEC 55P61 cross hot-wire probe. A DANTEC 90P20 thermometer was used to monitor temperature changes during measurements. The distance between the hot-wire probe, that is, the measuring points, and the holder was 250 mm. This distance is large enough that the effects of the flow distortion induced by the holder onto the measuring points are negligible. The hot-wire sensor diameters were 5 $\mu$m, and the active sensor lengths were 1.25 mm, giving a length-to-diameter ratio of 250. The hot-wire probes were connected to two DANTEC 90C10 constant temperature anemometers. The hot-wire system was continuously checked for resistance drift. The square wave test indicated that the frequency response for the cross hot wires was greater than 60 kHz. The hot-wire probes were calibrated via a DANTEC 90H10 calibration system. A fourth-order polynomial was used for the zero angle velocity calibration,[21] whereas for the yaw angle calibration the constant longitudinal cooling coefficient method $k^2$ was applied. The hot-wire velocity calibration relative errors, associated with the experimental uncertainty in instantaneous velocity measurements, were less than 0.5% in the cooling velocity calibration, less than 1% in the longitudinal component $u$, less than 10% in the lateral component $v$, and less than 10% in the Reynolds shear stress. For all three configurations, signals were sampled at 6 kHz for 60 s that gave approximately 3000 measured shedding periods. Statistical uncertainties of the longitudinal mean velocity are at most 0.3%, with a 95% confidence level. Statistical uncertainties[22] for the normal turbulence intensities are not more than 4.5%, with the same 95% confidence level. The voltages were offset and amplified with a gain of four and low-pass-filtered at 3 kHz using a 12-bit A/D board and stored on hard drives. The overheat ratio was set to 1.8. Linear temperature corrections were applied to voltages to compensate for the differences in temperature between calibration and the experiment.

Measurements were taken in the wake of the four wake generators described earlier at the following downstream $x/d$ and lateral $y/d$ positions: $(x/d, y/d) = \{(2, 2), (9, 0), (16, 0), (25, 0), (36, 0), (49, 0)\}$. Note that the first position is in the near wake, at the same location as in Ref. 12, whereas the others are in the intermediate to far wake. The first position was chosen to investigate the mitigation of the von Kármán vortex, whereas the others were considered to explore the farther downstream wake decay. For the wavy cylinders, wake measurements were taken at two spanwise locations that correspond to a peak and a valley of the sinusoidal perturbations (Fig. 1), whereas for the base case only one wake spanwise location was considered at the midspan.

## III. Results

### A. Near Wake

The effect of sinusoidal perturbations is investigated based on spectral analysis of the streamwise $u$ and lateral velocity $v$ fluctuations and using second-order turbulence statistics at $(x/d, y/d) = (2, 2)$. Power spectral density functions (PSD) of the $v$ component at valley and peak waviness locations are presented in Fig. 3 and correspond to the four analyzed configurations W0, W1, W2 and W3. Tables 1 and 2 show the normal $u'/U_0$ and the lateral $v'/U_0$ turbulence intensities, respectively, along with the turbulence intensity reduction parameters caused by the waviness, as referenced to the base case.

The PSD suggest that the three wavy cylinders configurations have three different flow characteristics that interestingly correspond to the three laminar flow regimes defined in Ref. 4. Thus, the PSD of the smallest wave steepness configuration $W1$ shows no qualitative changes from the base case, along with a negligible reduction of up to $9.8 \pm 4.5\%$ in the turbulence intensities (Tables 1 and 2).

The PSD of the second configuration W2 does show some qualitative changes from the straight case at the peak of the waviness. Moreover, a reduction in the turbulence intensity of up to $26 \pm 4.5\%$ at the valley and a small reduction of only $7.5 \pm 4.5\%$ at the peaks are found. Note that the reduction at the valleys takes place only at small scales, a phenomenon that needs further investigation. Also, it can be observed that the shedding frequency is the same as in the straight cylinder case regardless of the spanwise position, that is, waviness peak or valley. The Strouhal number based on this frequency, $Sr = fd/U_0$, is 0.139 and is in agreement with previous straight cylinders investigations.[23] Note that a first harmonic peak is present in the PSD in Figs. 3a–3c, but with a magnitude of about two orders less than the peak corresponding to the fundamental harmonic. The existence of the first harmonic peak in the spectra can be attributed to slight radial asymmetry of the shed vortices close to the generator. Also note that the Strouhal numbers are similar for both peak and valley locations. This indicates that there is no frequency-beating phenomenon as reported in Ref. 4 for the laminar regime 2 and in Ref. 12 for high Reynolds numbers. However, note that the frequency-beating phenomenon was found in the

**Table 1 Streamwise turbulence intensities at $(x/d, y/d) = (2, 2)$**

| Configuration | $(u'/U_0)_{\text{peak}}$ | Reduction at peak, % | $(u'/U_0)_{\text{valley}}$ | Reduction at valley, % |
|---|---|---|---|---|
| Standard | 17.16 | N/A | 17.16 | N/A |
| Wavy W1 | 16.07 | 6.70 | 15.78 | 8.40 |
| Wavy W2 | 16.18 | 6.13 | 13.068 | 23.97 |
| Wavy W3 | 8.50 | 50.72 | 3.94 | 76.96 |

**Table 2 Lateral turbulence intensities at $(x/d, y/d) = (2, 2)$**

| Configuration | $(v'/U_0)_{\text{peak}}$ | Reduction at peak, % | $(v'/U_0)_{\text{valley}}$ | Reduction at valley, % |
|---|---|---|---|---|
| Standard | 17.42 | N/A | 17.42 | N/A |
| Wavy W1 | 16.08 | 8.02 | 15.78 | 9.80 |
| Wavy W2 | 16.19 | 7.47 | 12.91 | 26.00 |
| Wavy W3 | 10.46 | 40.27 | 3.77 | 78.36 |

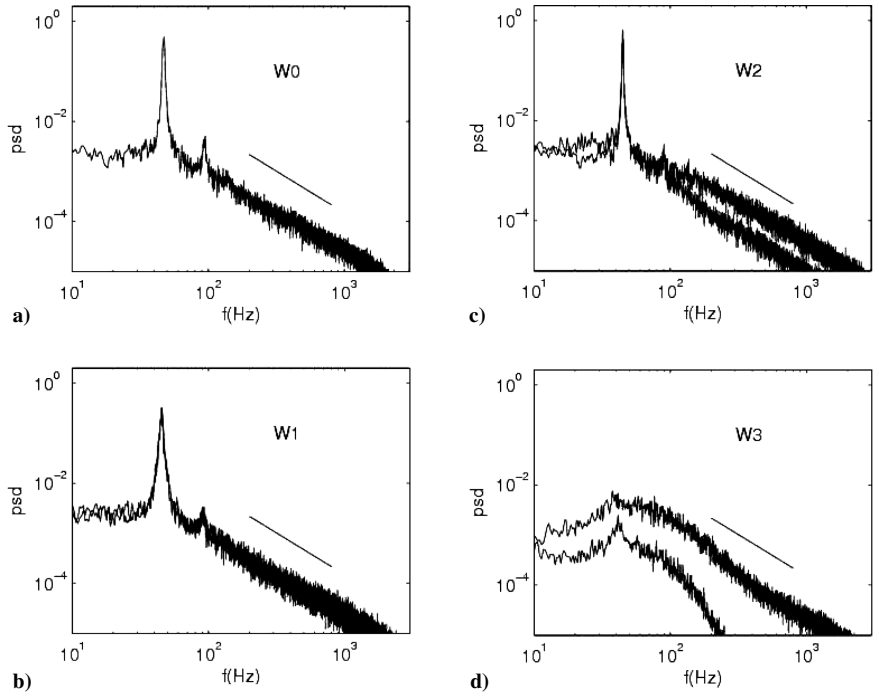


**Fig. 3 PSD at $(x/d, y/d) = (2, 2)$ at peak and valley locations for four configurations, W0, W1, W2, and W3; note that higher reductions correspond to valleys and that straight lines indicate the $-\frac{5}{3}$ slope.**

laminar case only for high spanwise wavelengths, $\lambda/d \geq 5.6$. Therefore, it can be conjectured that this might be a characteristic of the high spanwise wavelengths and does not occur at lower spanwise wavelengths.

The PSD of configuration W3 indicates a major weakening of the vortex shedding, similar to the laminar regime 3. The measurements at the waviness valley indicate again a strong inhibition of smaller flow scales. Also note that the reduction in turbulence intensities is $78 \pm 4.5\%$ at the valley and up to $50 \pm 4.5\%$ at the peak (Tables 1 and 2).

The qualitative similarity with the laminar results is important because the three configurations were chosen intentionally to correspond to three different laminar flow regimes, 1, 2, and 3, defined in Ref. 4. Figure 2 shows that the three wavy cylinder configurations precisely correspond to the three different low Reynolds number regimes in the $(w/\lambda, \lambda/d)$ plane. Note that Fig. 2 also shows the wavy cylinder configurations of Ref. 12 that correspond to larger spanwise wavelengths and all configurations in the laminar regime 3.

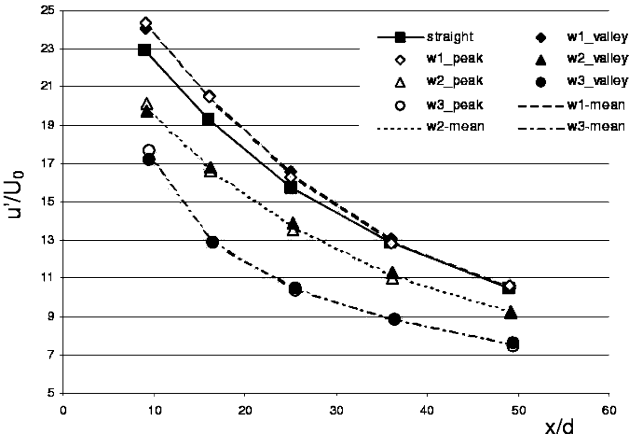


**Fig. 4 Downstream evolution of longitudinal turbulence intensity $u'/U_0$.**

### B. Wake Decay

The wake decay analysis was based on the investigation of the downstream evolution of the second-order turbulence statistics and on the PSD at five wake centerline locations: $(x/d, y/d) = \{(9, 0), (16, 0), (25, 0), (36, 0), (49, 0)\}$. Figure 4 shows the downstream evolution of the streamwise turbulence intensity $u'/U_0$ for the four investigated generators at peak and valley waviness locations. As a first observation, note that Fig. 4 indicates no difference between the two spanwise locations, this being an indication that the wake is statistically homogeneous in this direction. Note that in the near wake the spanwise geometrical variation of the generator makes the flow locally inhomogeneous by fixing the locations of the flow instabilities. Also note that the effect of generator waviness is beneficial in the reduction of the streamwise turbulence intensity at all analyzed locations and that the reduction increases with wave steepness, the larger the reduction. Figure 5 shows the corresponding results for the lateral turbulence intensity $v'/U_0$. Here, the first two wavy configurations W1 and W2 do not show any effect on the wake downstream evolution, the differences from the straight configuration being within the uncertainty errors. However, the third wavy configuration W3 produces a significant decrease in the investigated wake parameter of approximate $25 \pm 4.5\%$. Thus, it can be inferred that a sinusoidal SPPM using a wavelength of $2.4d$ is beneficial for achieving faster wake decay as was previously conjectured.[19]

A qualitative picture of the downstream evolution of the von Kármán vortices is given by the PSD. Figures 6–9 show the downstream spectral evolution at the wake centerline for the configurations W0, W1, W2, and W3, respectively. Note that due to the spanwise homogeneity mentioned earlier, only the results taken at the spanwise peak locations are shown. Figures 6–9 show that only the wavy configuration W3 produces a qualitatively different downstream wake evolution, the first two configurations W1 and W2, producing almost identical results with the straight cylinder case, in agreement with the second-order statistics results. Configuration W3 generates much smaller and broader peaks in the PSD, an indication that the von Kármán vortices are weaker and have significant three-dimensional characteristics. This is probably due to the interactions with ribs, in formal agreement with what was previously suggested for the intermediate wake of straight cylinders in Ref. 19. Note that the vortex shedding process seems to reappear further downstream $(x/d \geq 9)$ for the W3 configuration. (In the near

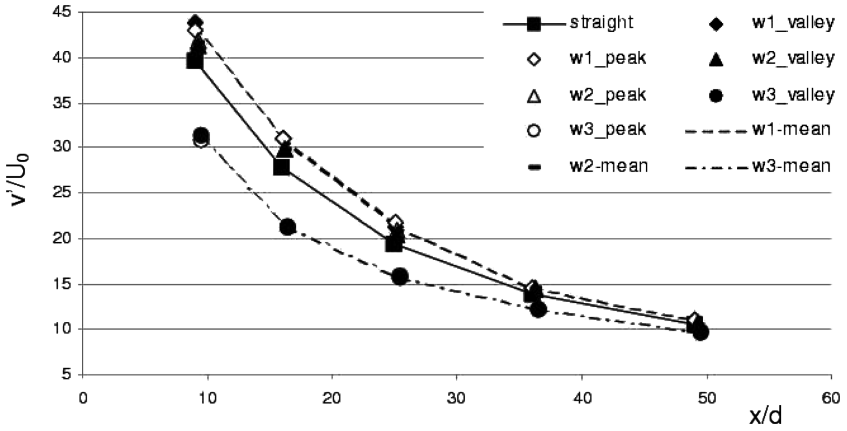


**Fig. 5 Downstream evolution of lateral turbulence intensity $v'/U_0$.**

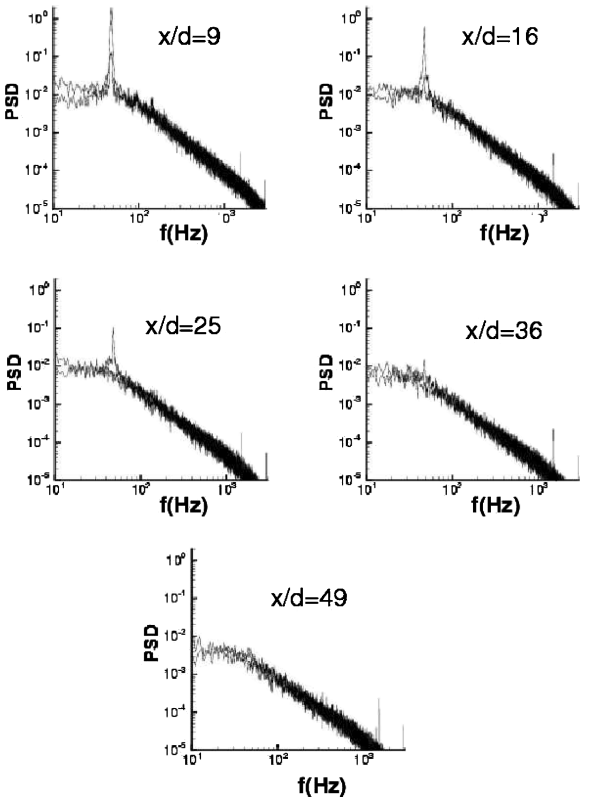


**Fig. 6 Straight cylinder, PSD of longitudinal *u* and lateral *v* velocity fluctuations; higher peaks correspond to *v* power spectra.**

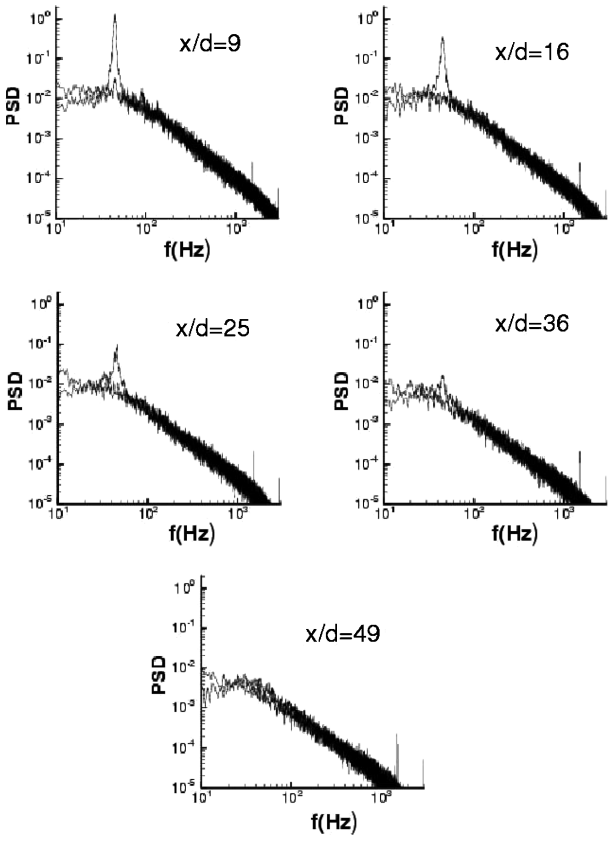


**Fig. 7 Wavy configuration W1, PSD of longitudinal *u* and lateral *v* velocity fluctuations; higher peaks correspond to *v* power spectra.**

wake we found that the vortex shedding was completely suppressed for this configuration.) The decay of the peak of the PSD seems to be slower. Similar results were observed for other types of control techniques, for example in-base bleeding and splitter plates, and could be attributed to a delay of the sequence of the absolute to the convective type of instabilities that generates the vortex shedding process.[17] However, it seems that for the present SSPM technique the reappearance of the vortex shedding is at a lower strength, which is beneficial for the wake control applications.

## IV. Discussions on the Relation Between Flow Topology and Control

The results presented in this paper suggest close similarities between the effect of the spanwise sinusoidal perturbations at low and high Reynolds numbers. This similarity implies that the wake three-dimensional transition mechanisms identified at low Reynolds numbers might apply to the high Reynolds numbers too. It is known that for low Reynolds numbers the wake three dimensionality is attained through two standard natural instability modes: mode *A* (Fig. 10a) and mode *B* (Fig. 10b). Both instability modes have von Kármán spanwise vortices as primary flow structures, shown as straight tubes along the *z* axis in Fig. 10, and ribs as streamwise secondary flow structures interconnecting the von Kármán vortices with different vorticity signs, that is, from both upper and lower sides of the wake in Fig. 10. The main topological difference between the two modes consists of a different streamwise vorticity sign alternation of ribs and in a different spanwise wavelength given by the spanwise arrangement of the ribs. These modes (*A* and *B*) have been identified in flow visualization at low Reynolds numbers for bluff-body and indented flat-plate wakes,[15,24] confirmed by numerical Floquet-based analysis[14,25] and by advanced experimental investigations based on particle image visualization.[26] However, debates still exist on the phenomenon responsible for triggering these modes.

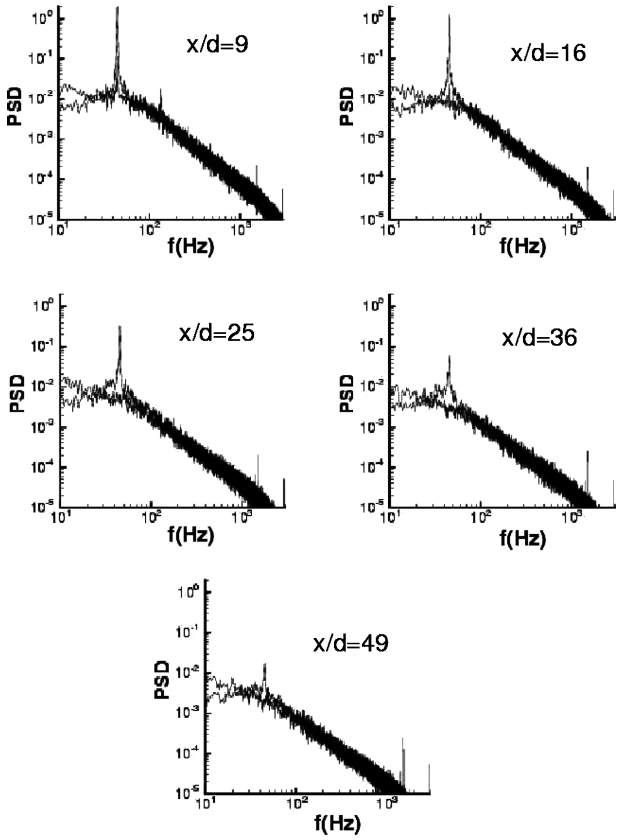


**Fig. 8 Wavy configuration W2, PSD of longitudinal *u* and lateral *v* velocity fluctuations; higher peaks correspond to *v* power spectra.**

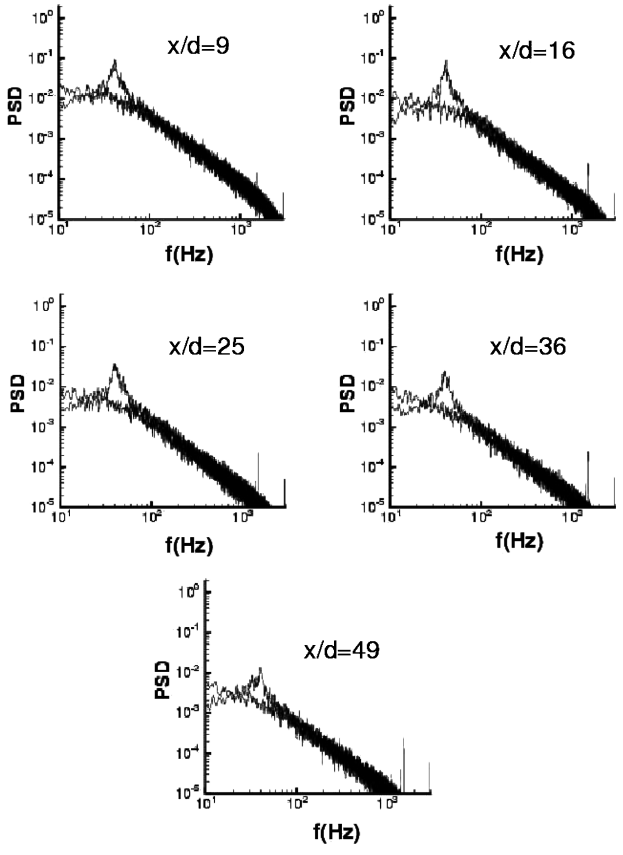


**Fig. 9 Wavy configuration W3, PSD of longitudinal *u* and lateral *v* velocity fluctuations; higher peaks correspond to *v* power spectra.**

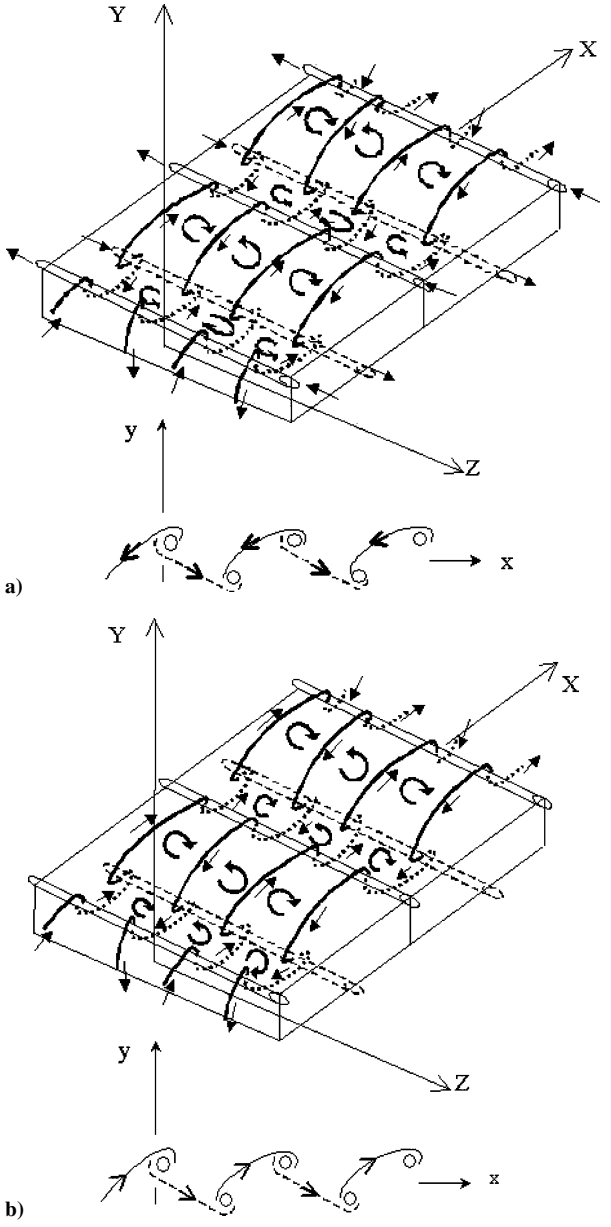


**Fig. 10 Two low-Reynolds-number instability modes: a) mode *A* and b) mode *B* (adaptation from Ref. 24).**

Based on simple two-dimensional stability analysis, it seems that the two modes are the result of two types of instabilities: elliptic for mode *A* and hyperbolic for mode *B* (Ref. 27). Another important observation is provided in Ref. 24, where it was indicated that mode *A* is triggered by vertical vorticity perturbations, for example, by indented flat plates, which that may be associated with the sinusoidal perturbation analyzed in this paper, and that mode *B* is triggered by horizontal vorticity perturbations, for example, by corrugated flat plates. What is important for control applications is that mode *A* seems to be more efficient in mitigating the spanwise vortices because it is related to elliptic instabilities that affect mainly the vortex core region. Therefore, this is the mode that should be triggered for control purposes. This observation is in agreement with studies showing that the efficiency of the sinusoidal perturbations relates to the triggering of the mode *A* that significantly affects the von Kármán vortices both in the near wake[4] and farther downstream.[19]

Therefore, for efficient wake control results, it is important to understand how to trigger mode *A*. Although, it has been shown that mode *A* could be excited by periodic vertical vorticity perturbations, for example, via spanwise indentations, sinusoidal geometric

perturbations, etc., the problem that remains unsolved is knowing the most unstable wavelength that should be excited. For flows over circular cylinders at low Reynolds number, it was shown that the most unstable spanwise wavelength $\lambda$ is 3–4$d$ (Ref. 15). It is also indicated in Ref. 15 that for a high Reynolds number the range of the unstable wavelengths becomes broader. These circular cylinder results can be extrapolated to other configurations because the spanwise $\lambda$ to streamwise $\lambda_x$ wavelength ratio seems to present a quasi-universal value, that is, 0.63–0.84 for mode $A$ (Ref. 19), and can be expressed as

$$\lambda/\lambda_x \approx \lambda/d \cdot Sr \tag{1}$$

Note that $d$ represents the generator transverse cross section ($Sr = fd/U_0$, with $f$ the shedding frequency and $U_0$ the freestream velocity). Later, Ref. 4 it is shown that at low Reynolds numbers, the square cylinders with sinusoidal faces have a broad range of most amplified wavelengths (Fig. 2). However, the most-unstable spanwise wavelength corresponds to the mode $A$ square cylinders, that is, 5.22$d$ found in Ref. 14. Note that by using Eq. (1) the mode $A$ wavelengths for square cylinders are between 4.5$d$ and 6$d$. Given the qualitative similarity between high and low Reynolds numbers showed herein, it could be inferred that the most-unstable wavelength for both laminar and turbulent regimes is approximate 5.2$d$, and, therefore, it should be the mode $A$ wavelength that has to be excited for control purposes when the reduction in both drag and unsteady loads are targeted. However, as mentioned herein, an optimum reduction of these two parameters does not necessary imply an optimization of the acceleration of the downstream wake decay.[16] Therefore, a different wavelength might need to be triggered for the latter parameter to be optimized as shown in the following text.

To investigate the most-unstable wavelength for the wake decay process, downstream wake evolution investigations should be performed. However, as we indicated, this has not drawn too much attention in the literature. Based on our knowledge, the only investigation of the spanwise wavelength influence on the wake downstream evolution was performed by Lasheras and Choi.[28] They obtained an interesting result indicating that there is no preferred natural spanwise wavelength for both-modes $A$ and $B$ at low Reynolds numbers and that the selection of a specific spanwise wavelength might be decided by the freestream conditions in different wind-tunnel facilities. For higher Reynolds numbers, the existence of a most-unstable wavelength is much more difficult to be established due to the difficulties encountered in obtaining accurate numerical results, assuring perturbation-free inlet conditions in experimental facilities and, moreover, due to the difficulties related to the interpretation of turbulence data. Note here the similarity between wakes and mixing layers. The mixing layer has at both high and low Reynolds numbers, a broad band of most amplified wavelength ratio $\lambda/\lambda_x$ centered at $\frac{2}{3}$ (found in both experimental and numerical studies[29,30]), interestingly, within the bounds of the universal wake mode $A$ wavelength range given by Eq. (1).

However, previous experimental investigations on square cylinder wakes at a high Reynolds number[19] indicate that, in the intermediate wake, there is a preferential spanwise wavelength of 2.4$d$ that gives a ratio of spanwise to streamwise wavelength of $\frac{2}{5}$, that is, lower than the range given by Eq. (1). Moreover, it has been confirm herein that a perturbation at this wavelength leads to faster wake decay. Nevertheless, considering the preceding discussions, we cannot state that our found wavelength is a natural most-unstable spanwise wavelength of the turbulent mode $A$ that is responsible for faster wake decay. This wavelength might also be related to the inlet conditions in our facility, similar to the mixing-layer debate, and, therefore, in the analysis of the optimum wavelength to produce the fastest wake decay the inlet conditions should also be taken in consideration. Moreover, that the wake outside the recirculation region is convectively unstable makes the similarity between the wake evolution and the mixing-layer characteristics justifiable. Thus, it is known that the convectively unstable flows are noise amplifiers and, therefore, that they become more dependent on the freestream conditions; it is from this point that the difficulties in finding the natural most-unstable wavelength emerge.

## V. Conclusions

Three different geometric sinusoidal perturbation amplitudes at a wavelength that corresponds to the intermediate wake instability mode $A$ ($\lambda = 2.4d$) are applied to the upstream faces of three square cylinders, and their effect is experimentally compared with a straight cylinder case.

Spectral analyses performed in the near wake, just outside of the formation region $(x/d, y/d) = (2, 2)$, indicate qualitative similarities between low and high Reynolds number flows, suggesting similar main flow dynamics. At the analyzed wavelength of 2.4$d$, three different flow regimes are identified for the high Reynolds number investigated herein, in agreement with the laminar case: regime 1 where no significant changes are noticed, regime 2 where decreases of approximately 26% in turbulence intensities at the waviness valley are recorded, and, finally, regime 3 where the vortex shedding is almost completely suppressed, the reductions in the turbulence intensities being up to 78%.

The downstream decay of the wake flow is also investigated at different downstream positions at the wake centerline, and it is shown that the sinusoidal perturbations at the wavelength corresponding to the instability mode in the intermediate wakes accelerate the wake decay. It is inferred, therefore, that this control method reduces the wake aeroelastic instabilities, too. However, it is shown that vortex shedding seems to reorganize itself further downstream, for $x/d \geq 9$, similar to the case of other flow control techniques, but at a low strength.

Given the relationship between flow topology and control methods, it is inferred that a wavelength of 5.2$d$, which corresponds to a universal wavelength $\lambda/\lambda_x = 0.66$, is the most-unstable wavelength that should be triggered when fluctuating lift and drag reductions are targeted, independent of the inlet conditions. When faster wake decay becomes the target, a wavelength of 2.4$d$, which corresponds to a universal wavelength $\lambda/\lambda_x = 0.4$ and is associated with the intermediate wake instability modes, seems to be very efficient. However, freestream conditions, that is, perturbation wavelength in the approaching inflow, might play an important role in establishing the most efficient wavelength to be excited for control purposes because in the wake decay process the natural instabilities might be overcome by the external freestream instabilities.

## Acknowledgments

This work was supported by Natural Science and Engineering Research of Canada Research Grants 166732 and 4282.

## References

[1]Fiedler, H. E., "Control of Free Turbulent Shear Flows," *Flow Control-Fundamentals and Practices*, edited by M. Gad-el-Hak, A. Pollard, and J.-P. Bonnet, Springer-Verlag, Berlin, 1998, pp. 335–429.

[2]Scruton, C., and Walshe, D. E. J., "A Means for Avoiding Wind-Excited Oscillations of Structures with Circular or Nearly Circular Cross Section," National Physical Lab., Aeronautical Rept. 335, Teddington, England, U.K., 1957.

[3]Bearman, P. W., and Branković, M., "Passive Control of Vortex-Induced Vibration," *Proceedings of the Conference on Bluff Body Wakes and Vortex-Induced Vibrations (BBVIV3)*, Office of Naval Research, U.S. Dept. of the Navy, Arlington, VA, and Office of Naval Research International Field Office, Melbourne, Australia, 2002, Paper 1.

[4]Darekar, R. M., and Sherwin, S. J., "Flow Past a Square-Section Cylinder with a Wavy Stagnation Face," *Journal of Fluid Mechanics*, Vol. 426, 2001, pp. 263-295.

[5]Naumann, A., Morsbach, M., and Kramer, C., "The Conditions of Separation and Vortex Formation past Cylinders," CP-4, AGARD, 1966, pp. 539–574.

[6]Tanner, M., "A Method of Reducing the Base Drag of Wings with Blunt Trailing Edges," *Aeronautical Quarterly*, Vol. 23, No. 1, 1972, pp. 15–23.

[7]Rodriguez, O., "Base Drag Reduction by the Control of Three-Dimensional Unsteady Vortical Structures," *Experiments in Fluids*, Vol. 11, No. 4, 1991, pp. 218–226.

[8]Petrusma, M. S., and Gai, S. L., "The Effect of Geometry on the Base Pressure Recovery of Segmented Blunt Trailing Edges," *Aeronautical Journal*, Vol. 98, No. 977, 1994, pp. 267–274.

[9]Petrusma, M. S., and Gai, S. L., "Bluff Body Wakes with Free, Fixed and Discontinuous Separations at Low Reynolds Numbers and Low Aspect Ratio," *Experiments in Fluids*, Vol. 20, No. 3, 1996, pp. 189–198.

[10]Bearman, P. W., and Tombazis, N., "The Effect of Three-Dimensional Imposed Disturbances on Bluff Body Near Wake Flows," *Journal of Wind Engineering and Industrial Aerodynamics*, Vol. 49, No. 1–3, 1993, pp. 339–350.

[11]Tombazis, N., and Bearman, P. W., "A Study of Three-Dimensional Aspects of Vortex Shedding from a Bluff Body with a Mild Geometric Disturbance," *Journal of Fluid Mechanics*, Vol. 330, 1997, pp. 85–112.

[12]Bearman, P. W., and Owen, J. C., "Reduction of Bluff-Body Drag and Suppression of Vortex Shedding by the Introduction of Wavy Separation Lines," *Journal of Fluids and Structures*, Vol. 12, No. 1, 1998, pp. 123–130.

[13]Vickery, B. J., "Fluctuating Lift and Drag on a Long Cylinder of Square Cross Section in a Smooth and a Turbulent Stream," *Journal of Fluid Mechanics*, Vol. 25, 1966, pp. 481–494.

[14]Robichaux, J., Balachandar, S., and Vanka, S. P., "Three-Dimensional Floquet Instability of the Wake of Square Cylinder," *Physics of Fluids*, Vol. 11, No. 3, 1999, pp. 560–578.

[15]Williamson, C. H. K., "Vortex Dynamics in the Cylinder Wake," *Annual Review of Fluid Mechanics*, Vol. 28, 1996, pp. 477–539.

[16]Monkewitz, P. A., "Wake Control," *Bluff-Body Wakes, Dynamics and Instabilities*, Springer-Verlag, Berlin, 1993, pp. 227–240.

[17]Patnaik, B. S. V., and Wei, G. W., "Controlling Wake Turbulence," *Physical Review Letters*, Vol. 88, No. 5, 2002, pp. 1–4.

[18]Thiria, B., Cadot, O., Goujon-Durand, S., Pradal, D., and Wesfried, J. E., "Forced Vortex Shedding and Control in Wakes," *Bulletin of the American Physical Society*, Vol. 48, No. 10, 2003, p. 108.

[19]Dobre, A., and Hangan, H., "Investigation of the Three-Dimensional Intermediate Wake Topology at High Reynolds Number," *Experiments in Fluids*, Vol. 37, No. 4, 2004, pp. 518–530.

[20]Dobre, A., "Investigations of the High Reynolds Number Bluff Bodies," Ph.D. Dissertation, Faculty of Engineering, Univ. of Western Ontario, London, ON, Canada, June 2003.

[21]Bruun, H. H., *Hot-wire Anemometry—Principles and Signal Analysis*, Oxford Univ. Press, Oxford, 1995, pp. 99–101.

[22]Benedict, L. H., and Gould, R. D., "Towards Better Uncertainty Estimates for Turbulence Statistics," *Experiments in Fluids*, Vol. 22, No. 2, 1996, pp. 129–136.

[23]Lyn, D. A., Einav, S., Rodi, W., and Park, J.-H., "A Laser-Doppler Velocimetry Study of Ensemble-Averaged Characteristics of a Turbulent Near Wake of a Square Cylinder," *Journal of Fluid Mechanics*, Vol. 304, 1995, pp. 285–319.

[24]Meiburg, E., and Lasheras, J. C., "Experimental and Numerical Investigation of the Three-Dimensional Transition in Plane Wakes," *Journal of Fluid Mechanics*, Vol. 190, 1988, pp. 1–37.

[25]Henderson, R. D., "Nonlinear Dynamics and Pattern Formation in Turbulent Wake Transition," *Journal of Fluid Mechanics*, Vol. 352, 1997, pp. 65–112.

[26]Brede, M., Eckelmann, H., and Rockwell, D., "On Secondary Vortices in the Cylinder Wake," *Physics of Fluids*, Vol. 8, No. 8, 1996, pp. 2117–2124.

[27]Thompson, M. C., Leweke, T., and Williamson, C. H. K., "The Physical Mechanism of Transition in Bluff Body Wakes," *Journal of Fluids and Structures*, Vol. 15, No. 3–4, 2001, pp. 607–616.

[28]Lasheras, J. C., and Choi, H., "Three-Dimensional Instability of a Plane Free Shear Layer," *Journal of Fluid Mechanics*, Vol. 189, 1988, pp. 53–86.

[29]Bernal, L. P., and Roshko, A., "Streamwise Vortex Structure in Plane Mixing Layers," *Journal of Fluid Mechanics*, Vol. 170, 1986, pp. 499–525.

[30]Rogers, M. M., and Moser, R. D., "Spanwise Scale Selection in Plane Mixing Layer," *Journal of Fluid Mechanics*, Vol. 247, 1993, pp. 321–337.

S. Aggarwal
*Associate Editor*